Modelling of geogrid-reinforced ballast under direct shear and impact loading

Ngoc Trung Ngo, Buddhima Indraratna, FASCE, & Fernanda Bessa Ferreira
University of Wollongong, Australia

ABSTRACT: Railways provide an efficient and economic transport mode in many parts of the developed countries including Australia, China, South Korea and the USA. Ballast layer is designed as a load bearing layer for rail tracks and to be free draining, but when the ballast voids are wholly or partially impeded due to the intrusion of fine particles or ballast breakage, the ballast can be considered to be fouled. Ballast degradation causes a reduction in the drainage capacity of ballast, thereby reducing the track resiliency and triggering high maintenance costs. Geosynthetics are commonly used in railway construction for reinforcement and stabilisation purposes. When railway ballast becomes degraded, the beneficial effect of geosynthetics could significantly decrease. A series of drop-weight impact tests and direct shear tests for ballast with and without the inclusion of geosynthetics are carried out in the laboratory. Discrete element modelling (DEM) is also carried out on ballast with and without the inclusion of geogrids. Load-deformation and ballast breakage responses obtained from the DEM simulations are in reasonable comparison with those measured experimentally. The research outcomes of this study can provide a fundamental laboratory and computational framework to assist practicing engineers in track design considering the role of geosynthetic inclusions.

Keywords: Ballast, Geogrids, Discrete Element Method, Railway

1 INTRODUCTION

Ballasted railway systems in Australia are heavily relied upon for the safe and efficient transportation of passengers and freight (Indraratna *et al.* 2013). The ballasted railway is typically divided into two key components: superstructure and substructure. The superstructure consists of the rails and sleepers, lying atop the substructure containing a ballast layer, sub-ballast layer and subgrade. The ballast layer is expected to adequately support rail superstructure by resisting lateral forces, reduce the transmission of stresses to lower levels and provide sufficient drainage (Selig and Waters, 1994, Indraratna *et al.* 2011a, Ngo *et al.* 2017a). Ballast is a hard, angular material typically consisting of high quality igneous, metamorphic or well cemented sedimentary rocks. A good quality ballast material should possess high shear strength, high toughness and resistance to weathering (Indraratna *et al.* 2011b, Biabani *et al.* 2016a). Such a heavy reliance on Australian railway networks to meet increasing passenger and freight demands has led to the generation of severe impact loadings. Impact loads are forces of high energy caused by wheel and rail abnormalities, such as worn rail surfaces, wheel flats and misaligned rail joints (Remennikov and Kaewunruen 2014). Regions of abrupt track stiffness change such as bridge and rail-road crossings commonly incur significant impact forces and inevitable ballast failure. Breakage, lateral movement, fouling and differential settlement are all common failure modes of ballast under increased traffic loading resulting in costly track maintenance and replacement (Tutumluer *et al.* 2012, Ngo and Indraratna 2016).

Past research has attempted to use cellular reinforcement (geocells) to provide lateral confinement to infill granular aggregates (Biabani *et al.* 2016b). Under induced loads, this additional confinement by the geocell helps to prevent infilled granular aggregates from spreading laterally, and by increasing infill

rigidity, geocells also improve the load-carrying capacity of track embankments, which in turn enhances track performance (Raymond 2002, McDowell *et al.* 2006, Ngo *et al.* 2016, among others). Planar geosynthetics have also been widely used to reinforce ballasted tracks and to increase the duration of track serviceability (McDowell and Stickley 2006, Fernandes *et al.* 2008, Qian *et al.* 2010, Indraratna *et al.* 2016, Ngo *et al.* 2017b, among others). It has been reported that the mechanical interlock by geosynthetics with ballast aggregates can reduce the lateral displacement and degradation of ballast, but despite these obvious benefits, current literature on the interface behaviour of geogrid-ballast is still limited, both in experimental studies and numerical simulations, particularly when ballast becomes fouled (Indraratna et al. 2011b, Ngo et al. 2017c). In this paper, the role of geosynthetics in stabilising coal-fouled ballast is described using a series of large-scale laboratory direct shear tests and discrete element modelling.

2 LABORATORY INVESTIGATION

2.1 *Large-scale direct shear test*

The large-scale direct shear apparatus used in this study consists of a 300mm × 300 mm^2 steel box, 200 mm high (Figure 1a). Ballast collected from Bombo quarry, New South Wales, Australia was cleaned and sieved according to Australian Standards (AS 2758.7, 1996). The recommended particle size distribution of ballast proposed by Indraratna et al. (2011a) for Australian rail tracks with a mean particle size of d_{50}=35mm was used in the current tests. Particles of ballast were sieved, weighed and thoroughly mixed to capture the desired grain size distribution and this grading conformed to the gradation limit specified in the Australian Standards. The coal fines are used as fouling contaminant and the Void Contamination Index (*VCI*) introduced earlier by Tennakoon *et al.* (2012) is applied to measure the degree of fouling, as follows:

$$VCI = \frac{1+e_f}{e_b} \times \frac{G_{sb}}{G_{sf}} \times \frac{M_f}{M_b} \times 100 \quad (1)$$

where e_f: the void ratio of fouling material; e_b: the void ratio of fresh ballast; G_{sb}: the specific gravity of ballast; G_{sf}: the specific gravity of fouling material; M_f: the dry mass of fouling material; M_b: the dry mass of fresh ballast. Coal fines were used as a fouling material for the *VCI*s of 20%, 40%, 70% and 95%. These amounts correspond to 5%, 10%, 18% and 25% of the weight of fresh ballast, respectively.

The particle size distribution of the materials used in the laboratory is presented in Figure 1b. While the testing programme and detailed results were discussed by Indraratna et al. (2011b), some of this data is used to compare with the DEM analysis presented later in this paper. In summary, the laboratory results show that the peak shear stress increases non-linearly with an increase of normal stress, but decreases as the *VCI* increases. This is attributed to coal fines coating the surface of ballast particles, thereby reducing the interlocking effect among grains. In other words, the coal fines fill the ballast voids to act as a lubricant, thereby facilitating the ballast particles to slide and roll over each other, resulting in increased dilation. Similar stress-strain behaviour of fouled ballast has also been experimentally observed by Huang et al. (2009).

2.2 *Behaviour of geogrid-reinforced ballast under impact loading*

Railway track structures are often subjected to impact forces due to irregularities in either a rail or a wheel, including wheel flats and out of round wheels, dipped rails, rail corrugation, defective rail welds, insulation joints and the expansion gap between two rail segments. Furthermore, at stiffness transitions zones, such as bridge approaches, tunnels and road crossings, large impact forces can also be generated leading to exacerbated deterioration of the track elements, with direct implications on track longevity (Indraratna 2016; Li and Davis 2005, Ferreira and Indraratna 2017). In this study, a high-capacity drop-weight impact testing equipment (Figure 2a) developed by Kaewunruen and Remennikov (2010) at the University of Wollongong, was used to investigate the mechanical response of railway ballast under impact loading and to assess the effectiveness of a biaxial geogrid (Figure 2b) in attenuating impact-induced damage. The test device consists of a 5.81 kN weight drop hammer that can be released from a maximum height of 6 m, resembling actual track conditions. The hammer is connected to rollers and is guided through low-friction runners on vertical steel columns fixed to a high-strength concrete floor. The equipment can accommodate test samples within a working area of 1500 × 1800 mm. The impact forces

are monitored by a dynamic load cell (capacity of 1200 kN) mounted on the drop hammer and connected to a computer controlled data acquisition system.

Figure 2c presents the schematic illustration of a typical test sample. To simulate a relatively low lateral confining pressure in the field, the ballast and subballast materials were confined in a cylindrical rubber membrane thick enough to avoid piercing by sharp ballast particles. First, a 150 mm thick subballast layer consisting of a mixture of gravel and sand was compacted in dry conditions to an initial unit weight of 18.8 kN/m^3. The ballast aggregates, consisting of fresh latite basalt from Bombo quarry (NSW, Australia), with a particle size distribution meeting the recommendations of AS 2758.7 (Standards Australia 1996), were thoroughly cleaned, sieved, mixed in required proportions and then compacted on the top of the subballast mass to a representative field unit weight of 15.3 kN/m^3, using an electric vibratory hammer. For comparison purposes, tests were performed with and without geogrid reinforcement. As shown in Figure 2c, the geogrid placement location within the test sample was varied (i.e., either at the base of the ballast layer or at 100 mm or 200 mm height) to analyse its possible influence on the ballast behaviour during impact loading. The biaxial geogrid (GGR) used in this study is composed of flat polypropylene bars with welded junctions and 31 mm square apertures, with a peak tensile strength of 40 kN/m and corresponding elongation of 8% (from manufacturer specifications).

The free-fall hammer was positioned at the required drop height (150 mm) and released through an electronic quick release system. The drop height was selected to generate dynamic stresses similar to those induced by wheel-flats and dipped rail joints in the field (Indraratna et al. 2010, Jenkins et al. 1974). For data recording purposes, an automatic triggering was enabled using the signal obtained during the hammer free-fall and the acquisition frequency was set to 50,000 Hz. The permanent vertical and lateral strains of the test samples after each impact were estimated by manual measurements at pre-established locations. The tests were discontinued after twelve impact blows due to the attenuation of ballast strains.

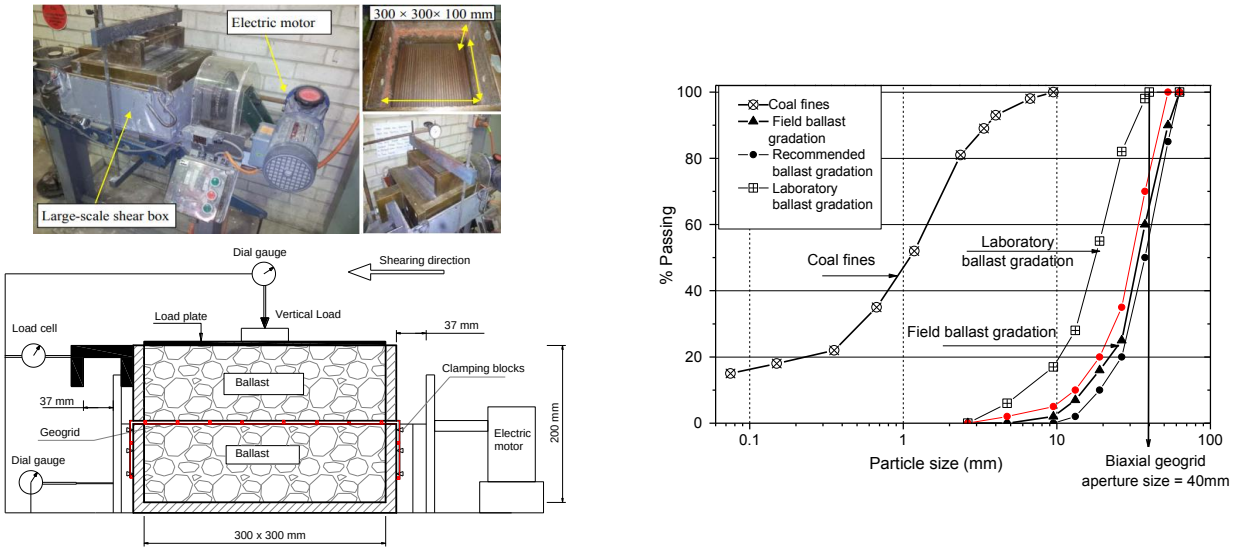

Figure 1. (a) Large-scale direct shear apparatus; (b) particle size distribution of tested materials

Figure 3a illustrates the typical impact force-time history under a single impact blow (first drop of the free-fall hammer) where distinct types of force peaks can be identified: multiple instantaneous sharp peaks and a much longer duration gradual peak of lower magnitude. The British Rail researchers designated these forces as P_1 and P_2, respectively (Jenkins et al. 1974), the terminology that is now widely used by track engineers. The impact forces P_1 are attributed to the inertia of the top plate resisting the downward movement of the drop hammer and lead to the compression of the contact zone between the drop hammer and the sample top plate. The effects of these forces are mostly filtered out by the load assembly, and therefore they do not have a significant influence on the ballast degradation (Frederick and Round 1985). Conversely, the peak force P_2 prevails over a longer duration and its occurrence is related to the mechanical resistance of ballast to impact loading. Hence, P_2 forces are of greater relevance in the analysis of track deterioration (Rochard and Schmid 2004), and should not exceed 322 kN in order to ensure track safety (British Rail Safety and Standards Board 1995).

The variation of P_2 forces with the number of blows along the different tests is plotted in Figure 3b, which shows a gradual increase of *P2* throughout the repeated impacts. The increase in the number of

blows causes the ballast to develop a denser packing assembly due to the rearrangement/reorientation and breakage of aggregates, which offers higher inertial resistance leading to an increased value of P_2. Figure 3b also suggests that the magnitude of P_2 forces is not significantly influenced by the presence or location of the geogrid reinforcement within the ballast assembly.

The permanent axial and radial strain responses of ballast along the tests conducted on unreinforced and geogrid-reinforced samples are presented in Figures 4a and 4b, respectively. These graphs show that ballast deformations increase progressively with the repeated impact blows, as expected. The strain increments are more pronounced during the initial impacts, due to the rearrangement and corner breakage of aggregates, and gradually reduce after a certain stage. Although the inclusion of a geogrid underneath the ballast layer (i.e., at the subballast-ballast interface) can considerably attenuate the ballast permanent deformations, in comparison to those in the absence of the reinforcement, higher efficiency is obtained when the geogrid is placed at 100 mm height from the subballast-ballast interface. The reduction in ballast strains as the location of the geogrid is changed from the base of the ballast mass to 100 mm above the subballast-ballast interface is attributed to an improved ballast-geogrid interlock, as the particles both above and below the geogrid can penetrate its apertures, as opposed to when the geogrid is installed directly above a dense subballast layer. However, when the reinforcement is installed at 200 mm height, its efficiency in mitigating the ballast permanent strains considerably decreases, which may be associated with considerable geogrid damage occurring when it is located close to the point of load application, as per the visual inspection of the geogrid sample after the test. In short, the optimum geogrid placement position as determined from the present study is 100 mm above the base of the ballast layer, provided that it will not interfere with ballast tamping and cleaning operations.

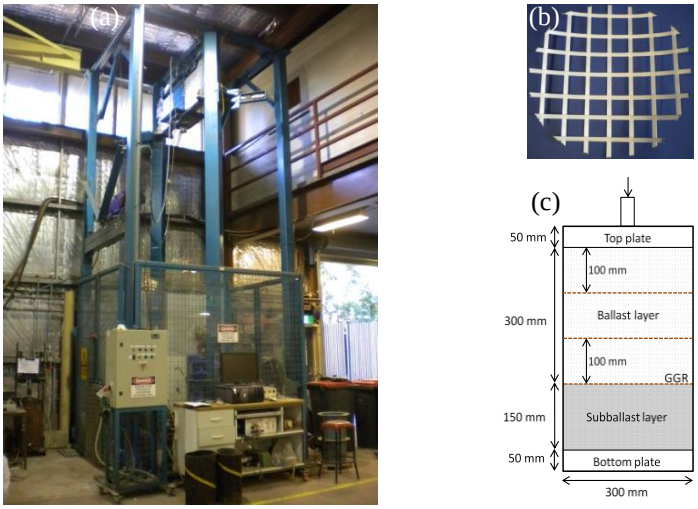

Figure 2. Details of the experimental programme: (a) Drop-weight impact test apparatus (Kaewunruen and Remennikov, 2010); b) geogrid sample; c) schematic illustration of a test sample

3 DISCRETE ELEMENT MODELLING OF GEOGRID-REINFORCED BALLAST

The discrete nature of railway ballast material leads to complex behaviour under traffic loading which cannot be adequately modelled through continuum methods (e.g. Finite Element Method or Finite Difference Method). The Discrete Element Method (*DEM*) has been increasingly used to study the behaviour of granular material both from macro-mechanical and micro-mechanical points of view (Cundall and Strack 1979). It enables to study some features of ballast, such as contact force distributions, particle displacement vectors, inter-particle friction and coordination number that are almost impossible to measure experimentally or using other numerical techniques (Potyondy and Cundall 2004, Lobo-Guerrero and Vallejo 2006, O'Sullivan 2011, Ngo *et al.* 2017d, among others). The dynamic behaviour of a granular assembly is simulated in the *DEM* by a time-stepping algorithm, utilising a central-difference scheme to integrate accelerations and velocities. The time-step in the *DEM* is generally selected so small that, during a single time-step, disturbances cannot propagate from any particle further than its immediate neighbours (Soga and O'Sullivan 2010, Ngo *et al.* 2017b). The irregular shapes of ballast particles can be realistically modelled in the *DEM* by connecting many spherical balls together using parallel bonds.

Moreover, an identically prepared ballast assembly can be reused for different loading and fouling conditions in the *DEM*.

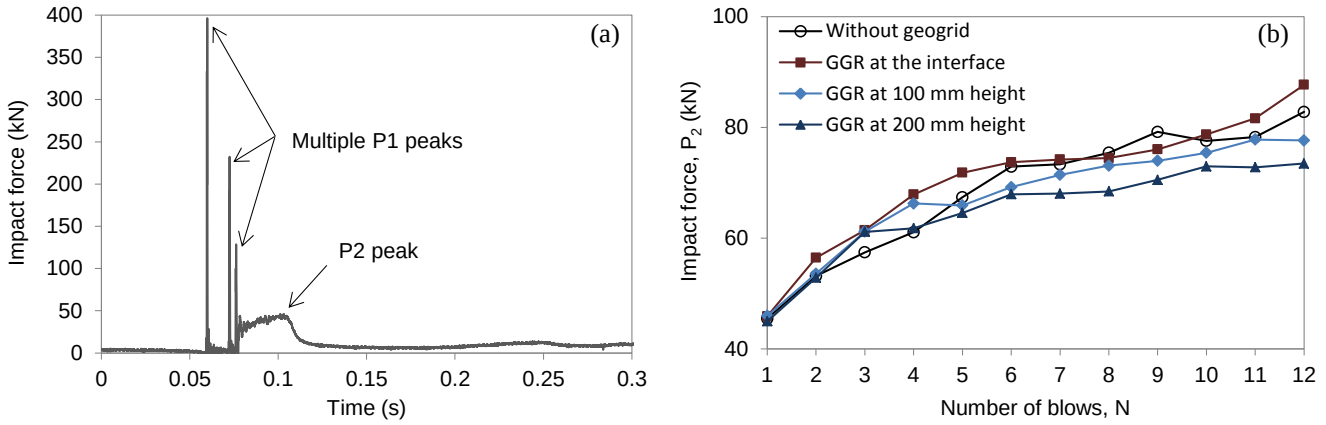

Figure 3. Impact force response: a) typical impact force-time history under a single impact blow; b) variation of impact force P2 with the number of blows for different test conditions.

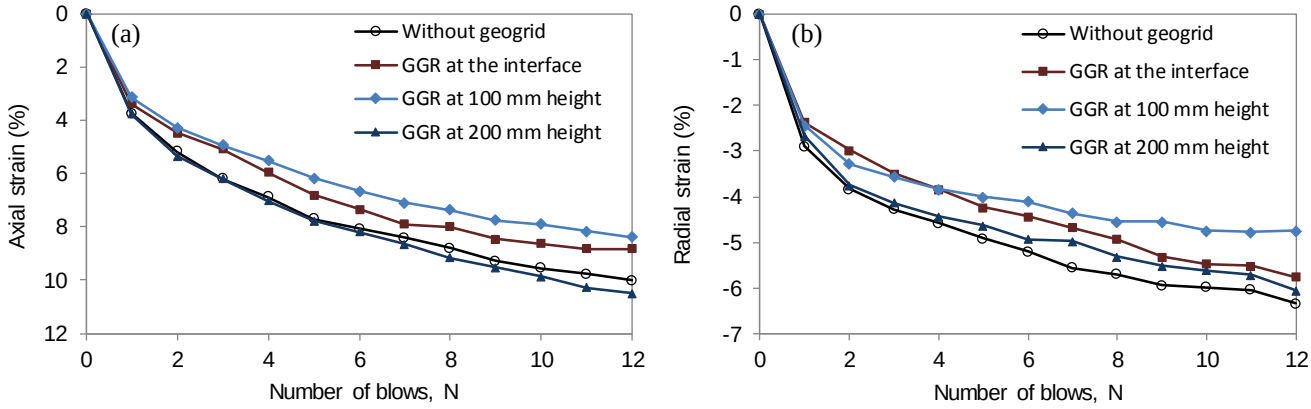

Figure 4. Variation of ballast permanent strains with the number of impact blows: a) axial strain; b) radial strain.

3.1 *Modelling of ballast, coal fines and geogrids in DEM*

The irregularity of ballast particles was modelled in this study by clumping many small spheres together, as depicted in Figure 5a. Small spheres were generated and overlapped together according to the configuration of an irregular particle. Typical particle shapes selected from real ballast aggregates were mimicked by assembling a number of spherical balls, as described earlier by Indraratna *et al.* 2014. A large-scale direct shear box (300mm long × 300mm wide × 200mm high) separated horizontally into two equal boxes was simulated using rigid walls. A free loading plate that allowed the particles to move vertically during shearing was placed on the top boundary. This plate was used to apply a normal load and monitor the normal displacement during shearing. A total of 8281 clumped particles having a particle size distribution similar to that of the ballast tested in the laboratory were generated in order to model the actual ballast gradation used in the experiments. Particles were placed in the shear box at random orientations to resemble experimental conditions. The void ratio of the assembly representing the initial condition of the test specimen was controlled at 0.82 (i.e. porosity of 45%), similar to the ballast samples used in the laboratory. The *DEM* simulation of this direct shear box for fresh ballast is shown in Figure 3b and a set of micro-mechanical parameters adopted for *DEM* simulation of fresh ballast are given in Table 1. A linear contact model, following previous studies, was used for the numerical simulations (e.g. McDowell *et al.* 2006, Lu and McDowell 2010, Ngo *et al.* 2014).

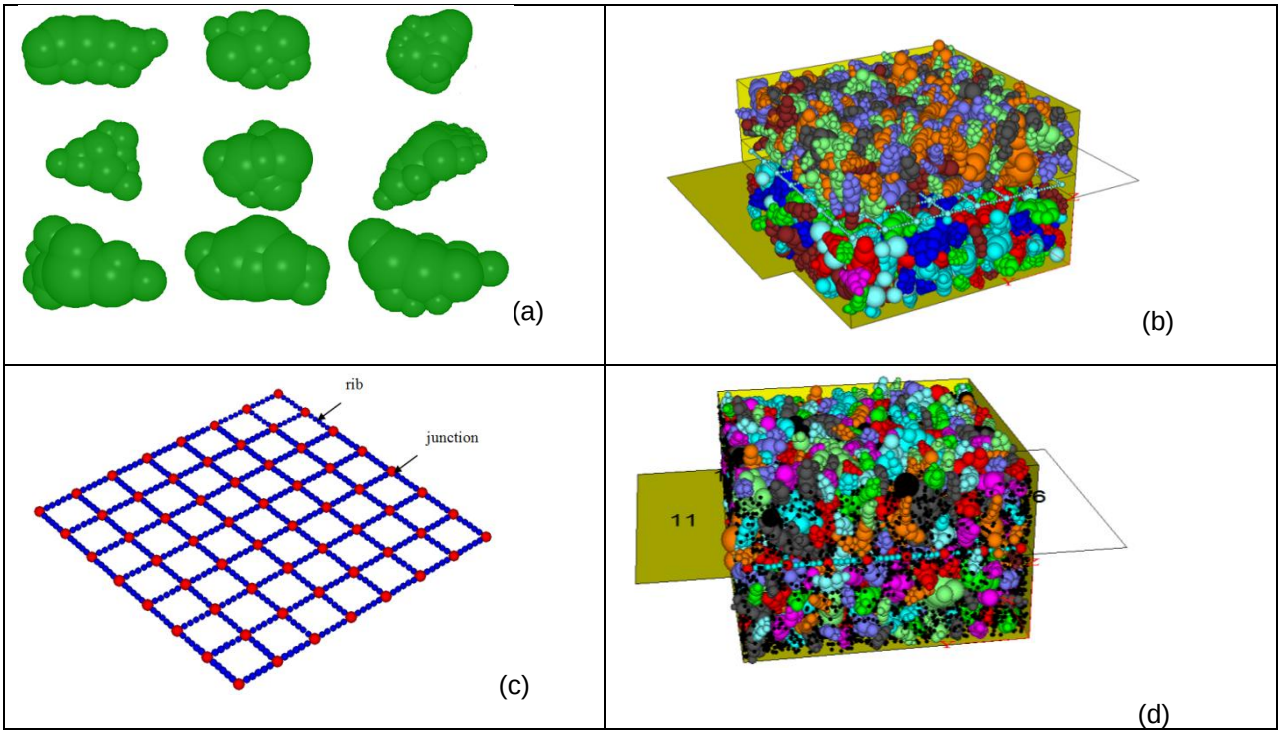

Figure 5. DEM model of geogrid-reinforced ballast: (a) simulated grains; (b) fresh ballast; (c) geogrid; and (d) fouled ballast (modified after Ngo et al. 2014)

Ballast fouling is caused by fine particles accumulated in the voids of ballast. Therefore, to be realistic, fouled ballast should be simulated in DEM by adding a different amount of fine particles into the ballast voids to represent different values of *VCI*. To simulate fouled ballast with *VCI*=40%, a predetermined number of 1.5mm spheres (e.g. 145,665 balls) was generated into the voids of fresh ballast. The values of normal and shear stiffness (k_n and k_s) required for the DEM analysis are generally difficult to determine correctly. In order to obtain some acceptable values of k_n and k_s, small scale shear box testing (60 × 60 × 25mm) was conducted on compacted coal fouling. By varying the k_n and k_s values in the DEM simulation to match the shear stress-strain plots obtained from direct shear testing, k_n=k_s=1.27x10^4 N/m was found to be appropriate. The relevant micromechanical parameters (k_n, k_s, μ) for coal fines are shown in Table 1.

A biaxial geogrid with an aperture size of 40 × 40 mm, similar to the geogrid tested in the laboratory was modelled by connecting numbers of spherical balls together. To approximately mimic the geogrid geometry, the geogrid was modelled by using bonded particles of 2.0mm radius at the ribs and 4.0mm radius at the junctions, as shown in Figure 5c. The contact bond strength and parallel bond strength between particles modelling the geogrid, corresponding to its tensile strength, were determined by tensile testing; and the geogrid micromechanical parameters are given in Table 1.

Table 1. Micromechanical parameters of geogrid, ballast and coal fines adopted in DEM simulation

Parameter	Ballast	Coal fines	Geogrid
Particle density (kg/m$^{3)}$	2700	800	800
Coefficient of friction	0.83	0.2	0.52
Contact normal stiffness, k_n (N/m)	0.52×10^8	1.27×10^4	1.77×10^7
Contact shear stiffness, k_s (N/m)	0.52×10^8	1.27×10^4	0.88×10^7
Contact normal stiffness of wall-particle, $k_{n\text{-wall}}$ (N/m)	1×10^8	1×10^8	1x10^8
Shear stiffness of wall of wall-particle, $k_{s\text{-wall}}$ (N/m)	1×10^8	1×10^8	1x10^8
Parallel bond radius multiplier, r_p			0.5
Parallel bond normal stiffness, k_{np} (kPa/m)			5.68×10^8
Parallel bond shears stiffness, k_{sp} (kPa/m)			5.68×10^8
Parallel bond normal strength, σ_{np} (MPa)			456
Parallel bond shear strength, σ_{sp} (MPa)			456

3.2 *Shear stress-strain and volumetric behaviour of fresh and fouled ballast*

A series of laboratory tests and DEM simulations for fresh and fouled ballast reinforced by geogrid was carried out at three normal stresses of 27kPa, 51kPa and 75kPa. Figure 6 shows comparisons of the shear stress-strain and volumetric responses of fresh and fouled ballast (*VCI*=40%) between the DEM

simulation and those measured experimentally. In general, the DEM results agree reasonably well with the experimental results at any given normal stress. The strain softening behaviour and volumetric dilation were also observed, such that at higher normal stresses, greater peak shear stresses and smaller dilation were captured, as expected. This strain softening behaviour of fresh ballast followed a similar trend to that of other rockfills of comparable sizes (e.g. Marsal 1973, Indraratna *et al.* 2017). Figure 6 shows that the DEM results deviate significantly from the laboratory data particularly around 4-7% of shear strain. This can be due to the limitations of the DEM model in exactly replicating the true angularity of the actual ballast grains and the fact that particle breakage has not been correctly modelled in this study. The presence of coal fines in the ballast assembly facilitated the reduced interlock between the ballast grains and geogrids which resulted in lower shear strength.

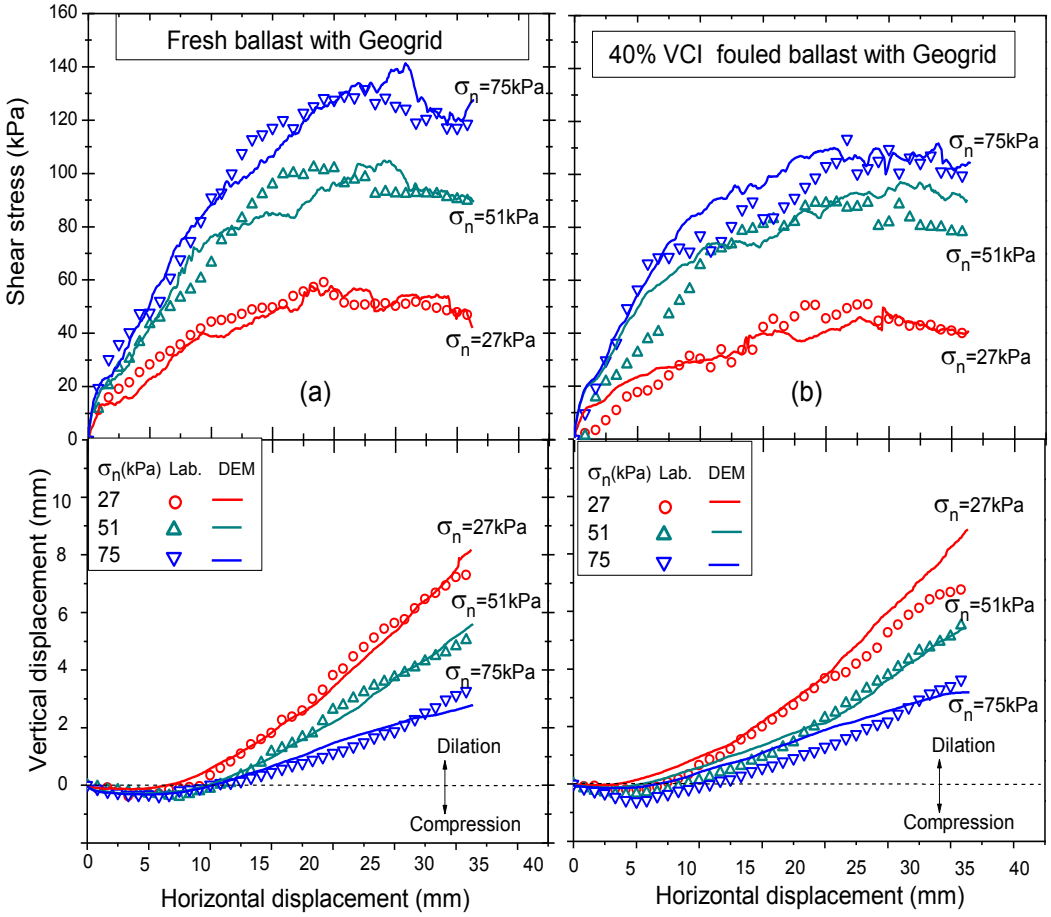

Figure 6. Comparisons of shear stress-strain and volumetric response of 40%*VCI*-fouled ballast between experiment and DEM simulation (data source from Ngo et al. 2014)

3.3 *Contours of strains developed in the geogrid*

Figures 7a and 7b present the contours of strain developed across the geogrid at the end of the shear test for fresh and 40%*VCI* fouled ballast, respectively. The simulated and actual deformed shape of the geogrid at the end of the test is also shown in Figure 7c-d. It can be seen that the strains developed non-uniformly across the geogrid and the magnitude of strain depended on the interlocking that occurred between the geogrid and ballast grains. The geogrid placed in the fresh ballast exhibited a slightly higher maximum strain than that in the 40%*VCI* fouled ballast (i.e., 1.4% strain in fresh ballast compared to 1.0% strain in 40%*VCI*-fouled ballast). This would be associated with the reduced interlocking effect of the geogrid and ballast aggregates due to coal fines which clog the interface between the ballast and the geogrid.

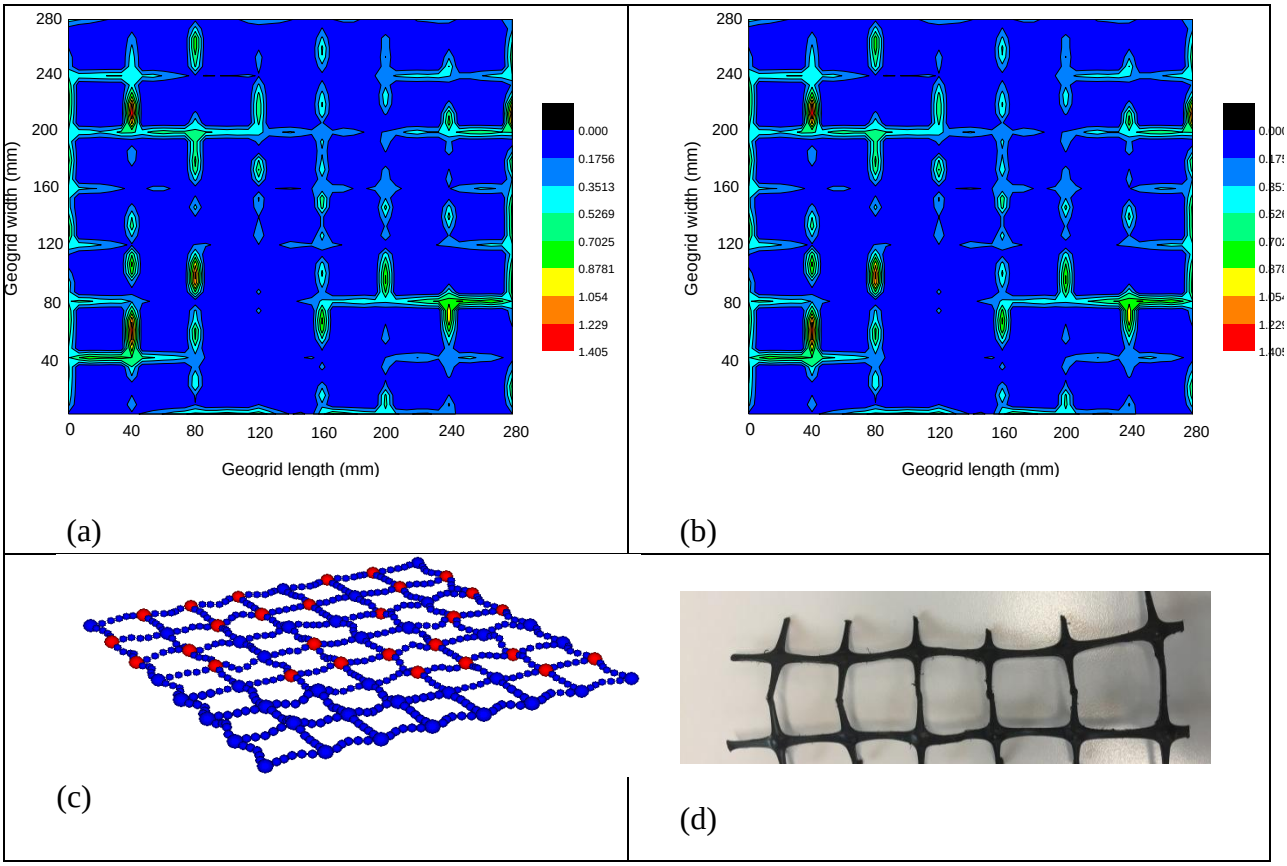

Figure 7. Contour strains developed across the geogrid at the end of test: (a) fresh ballast and (b) 40% *VCI* fouled ballast; (c) simulated deformed geogrid; and (d) image of deformed grid after test (modified after Ngo et al. 2014)

4 CONCLUSIONS

This paper presents the laboratory investigation and numerical modelling of geogrid-reinforced ballast under impact and direct shear loads. Under impact loading conditions, the use of a biaxial geogrid attenuated the lateral and vertical deformations of ballast and the particle breakage, and the highest efficiency was achieved when the geogrid was placed within the ballast layer, at 100 mm height from its base. This is associated with an enhanced ballast-geogrid interaction attained when the ballast particles on both sides of the geogrid can penetrate its apertures, as opposed to when the reinforcement is placed directly over a dense subballast mass. A series of experiments and DEM simulations of large-scale direct shear tests were carried out to study the stress-strain behaviour of fresh and fouled ballast (*VCI*=40%). The tests were conducted at three relatively low normal stresses of 27kPa, 51kPa, and 75kPa to simulate low confining pressure in rail tracks. For a given normal stress, the results obtained from the DEM analysis matched reasonably well with the data measured in the laboratory, indicating that this DEM model could capture the stress-strain behaviour of fresh and fouled ballast quite adequately. Based on the DEM simulation, the strains developed in the geogrid were also captured. The geogrid in 40%*VCI*-fouled ballast exhibited a slightly lower maximum strain than that in the fresh ballast, mainly because the fines accumulating in the ballast-geogrid interface reduced the interlock between them. The presence of coal fines in the ballast assembly facilitated the reduced interlock between the ballast grains and geogrid which resulted in lower interface shear strength. The research outcomes of this study can provide a fundamental laboratory and computational framework to assist practicing engineers in track design considering the role of geosynthetic inclusions.

ACKNOWLEDGEMENTS

The authors would like to thank the Rail Manufacturing CRC (Projects R2.5.1 and R2.5.2), Australasian Centre for Rail Innovation (ACRI), Tyre Stewardship Australia (TSA), Global Synthetics Pty Ltd, Naue GmbH & Co. KG and Foundation Specialists Group for the funding of this research. A significant portion of these contents was reproduced with kind permission from Computers and Geotechnics, Geotextiles and Geomembranes and International Journal of Geomechanics, ASCE. The laboratory assistance from technical officers Alan Grant, Cameron Neilson and Ritchie McLean is appreciated.

REFERENCES

Australia Standards (1996). Aggregates and rock for engineering purposes. Part 7: Railway ballast. AS 2758.7. Sydney, Australia.

British Rail Safety and Standards Board (1995). Commentary on permissible track forces for railway vehicles: Issue 1. GM/RC2513. Rail Safety and Standards Board, London, UK.

Biabani, M.M., Indraratna, B. and Ngo, N.T. (2016a). "Modelling of geocell-reinforced subballast subjected to cyclic loading." Geotextiles and Geomembranes, 44(4), pp: 489-503.

Biabani, M.M., Ngo, N.T. and Indraratna, B. (2016b). "Performance evaluation of railway subballast stabilised with geocell based on pull-out testing." Geotextiles and Geomembranes, 44(4), pp: 579-591.

Cundall, P.A. and Strack (1979). A discrete numerical model for granular assemblies. Geotechnique, 29(1), 47-65.

Ferreira, F.B. & Indraratna, B. (2017). Deformation and degradation response of railway ballast under impact loading – effect of artificial inclusions. Proceedings of the First International Conference on Rail Transportation, Chengdu, China, Paper ID:362.

Frederick, C.O. & Round, D.J. (1985). Vertical Track Loading. Track Technology, Thomas Telford, London, UK, pp. 135-149.

Fernandes, G., Palmeira, E.M. and Gomes, R.C. (2008). "Performance of geosynthetic-reinforced alternative sub-ballast material on a railway track." Geosynthetics International, 15(5), pp: 311-321.

Huang, H., Tutumluer, E. and Dombrow, W. (2009). "Laboratory characterisation of fouled railroad ballast behavior." Transportation Research Record: Journal of the Transportation Research Board, No. 2117, Washington, DC.

Kaewunruen, S. and Remennikov, A. M. (2010). "Dynamic crack propagations in prestressed concrete sleepers in railway track systems subjected to severe impact loads." Journal of Structural Engineering, 136(6), pp: 749-754.

Indraratna, B., Salim, W. and Rujikiatkamjorn, C. (2011a). Advanced Rail Geotechnology - Ballasted Track, CRC Press, Taylor & Francis Group, London, UK

Indraratna, B., Ngo, N.T. and Rujikiatkamjorn, C. (2011b). "Behavior of geogrid-reinforced ballast under various levels of fouling." Geotextiles and Geomembranes, 29(3), pp: 313-322.

Indraratna, B., Ngo, N.T. and Rujikiatkamjorn, C. (2013). "Deformation of coal fouled ballast stabilized with geogrid under cyclic load." Journal of Geotechnical and Geoenvironmental Engineering, 139(8), pp: 1275-1289.

Indraratna, B., Ngo, N.T., Rujikiatkamjorn, C. (2014). Behaviour of fresh and fouled railway ballast subjected to direct shear testing - a discrete element simulation. International Journal of Geomechanics,14(1), pp: 34-44.

Indraratna, B., Nimbalkar, S.S., Ngo, N.T. and Neville. (2016). Performance improvement of rail track substructure using artificial inclusions – Experimental and numerical studies. Transportation Geotechnics, 8, 69-85.

Indraratna, B. (2016). Railroad performance with special reference to ballast and substructure characteristics. 1st Proctor Lecture of ISSMGE, Transportation Geotechnics, Vol. 7, pp. 74-114.

Indraratna, B., Sun, Q., Ngo, N.T. and Rujikiatkamjorn, C. (2017). "Current research into ballasted rail tracks: model tests and their practical implications." Australian Journal of Structural Engineering, pp: 1-17.

Indraratna, B., Nimbalkar, S., Christie, D., Rujikiatkamjorn, C. & Vinod, J.S. (2010). Field assessment of the performance of a ballasted rail track with and without geosynthetics. Journal of Geotechnical and Geoenvironmental Engineering, ASCE, Vol. 136(7), pp. 907–917.

Jenkins, H. M., Stephenson, J. E., Clayton, G. A., Moorland, J. W. & Lyon, D. (1974). The effect of track and vehicle parameters on wheel/rail vertical dynamic forces. Railway Engineering Journal, Vol. 3(1), pp. 2-16.

Kaewunruen, S. & Remennikov, A. M. (2010). Dynamic crack propagations in prestressed concrete sleepers in railway track systems subjected to severe impact loads. Journal of Structural Engineering, 136(6), pp. 749-754.

Li, D. & Davis, D. (2005). The transition of railroad bridge approaches. Journal of Geotechnical and Geoenvironmental Engineering, Vol. 131(11), pp. 1392-1398.

Lobo-Guerrero, S. and Vallejo, L.E. (2006). "Discrete element method analysis of railtrack ballast degradation during cyclic loading." Granular Matter, 8(3-4), pp: 195-204.

Lu, M. and McDowell, G.R. (2010). "Discrete element modelling of railway ballast under monotonic and cyclic triaxial loading." Geotechnique, 60(6), pp: 459-467.

Marsal, R.J. (1973). Mechanical properties of Rockfill. In : Embankment Dam Engineering Wiley, New York.

McDowell, G.R., Harireche, O., Konietzky, H., Brown, S.F. and Thom, N.H. (2006). "Discrete element modelling of geogrid-reinforced aggregates." Proceedings of the ICE - Geotechnical Engineering 159(1), pp: 35-48.

McDowell, G.R. and Stickley, P. (2006). "Performance of geogrid-reinforced ballast." Ground Engineering, 1, 26.
Ngo, N.T., Indraratna, B. and Rujikiatkamjorn, C. (2014). "DEM simulation of the behaviour of geogrid stabilised ballast fouled with coal." Computers and Geotechnics, 55, pp: 224-231.
Ngo, N.T., Indraratna. (2016). Improved performance of rail track substructure using synthetic inclusions: Experimental and numerical investigations. International Journal of Geosynthetics and Ground Engineering, 2(3), pp: 1-16.
Ngo, N.T., Indraratna, B. and Rujikiatkamjorn, C. (2016). "Modelling geogrid-reinforced railway ballast using the discrete element method." Transportation Geotechnics, 8(2016), pp: 86-102.
Ngo, N.T., Indraratna, B. and Rujikiatkamjorn, C. (2017a). "Micromechanics-based investigation of fouled ballast using large-scale triaxial tests and discrete element modeling." Journal of Geotechnical and Geoenvironmental Engineering, 134(2), pp: 04016089.
Ngo, N.T., Indraratna, B. and Rujikiatkamjorn, C. (2017b). "Simulation Ballasted Track Behavior: Numerical Treatment and Field Application." International Journal of Geomechanics, 17(6), pp: 04016130.
Ngo, N.T., Indraratna, B. and Rujikiatkamjorn, C. (2017c). "Stabilisation of track substructure with geo-inclusions – experimental evidence and DEM simulation." International Journal of Rail Transportation, 5(2), pp: 63-86.
Ngo, N.T., Indraratna, B. and Rujikiatkamjorn, C. (2017d). "A study of the geogrid–subballast interface via experimental evaluation and discrete element modelling." Granular Matter, 19(3), pp: 54.
O'Sullivan, C. (2011). Particulate Discrete Element Modelling: A Geomechanics Perspective, Spon press, London.
Potyondy, D.O. and Cundall, P.A. (2004). "A bonded-particle model for rock." International Journal of Rock Mechanics and Mining Sciences, 41(8), pp: 1329-1364.
Qian, Y., Han, J., Pokharel, S.K. and Parsons, R.L. (2010). "Experimental study on triaxial geogrid-reinforced bases over weak subgrade under cyclic loading." GeoFlorida 2010: Advances in Analysis, Modeling & Design (Geotechnical Special Publication, 199), ASCE, pp: 1208-1216.
Raymond, (2002). Reinforced ballast behaviour subjected to a repeated load. Geotextiles and Geomembranes, 20(1).
Remennikov, A.M. and Kaewunruen, S. (2014). "Experimental load rating of aged railway concrete sleepers." Engineering Structures, 76, pp: 147-162.
Rochard, B.P. & Schmidt, F. (2004). Benefits of lower-mass trains for high speed rail operations. Proceedings of the Institution of Civil Engineers - Transport, Vol. 157(1), pp. 51-64.
Soga, K. and O'Sullivan, C. (2010) .Modeling of geomaterials behavior. Soils and Foundations, 50(6), 861-875.
Tutumluer, E., Huang, H. and Bian, X. (2012). "Geogrid-aggregate interlock mechanism investigated through aggregate imaging-based discrete element modeling approach." International Journal of Geomechanics, 12(4), pp: 391-398.